Detecting G4 unwinding

Stefan Juranek and Katrin Paeschke*
Department of Oncology, Hematology and Rheumatology, University Hospital Bonn, Bonn, Germany
*Corresponding author: e-mail address: katrin.paeschke@ukbonn.de

Contents

Abstract

DNA can, in addition to the B-DNA conformation, fold into a variety of additional conformations. Among them are G-quadruplex structures that have gained a lot of attention in recent years. G-quadruplex structures (G4s) are highly stable nucleic acid structures that can fold within DNA and RNA molecules. They form in guanine-rich regions that harbor a specific G4 motif. The three-dimensional structure forms via Hoogsteen hydrogen bonding, where the guanines form hydrogen bonds to each other in order to generate G quartets, which stack in order to become G4 structures.

The existence and relevance of G4s was controversial as discussed in the past. However, accumulating data was published that supported the model that G4s form in living cells and importantly support biological processes. G4 formation and unfolding is tightly regulated *in vivo*. If G4s persist in the cell, they can lead to cellular defects such as genome instability. To avoid G4 accumulation in cells, and by this prevent cellular defect, cells has evolved a variety of proteins, mostly helicases, that efficiently unfold G4 DNA and RNA structures. Here, we describe a detailed protocol to monitor G4 structure unfolding by helicases.

Methods in Enzymology
ISSN 0076-6879
https://doi.org/10.1016/bs.mie.2022.03.034

1. Introduction

The central dogma of molecular biology describes the propagation of genetic information from DNA to RNA to protein. Only in the last several years has it become obvious that this process is not linear. DNA and RNA molecules can directly influence this process and each other by the formation of alternative structures (Shapiro, 2009). In recent years, a variety of alternative DNA and RNA structures have been described in the literature (Wu & D'Souza, 2020). The formation of alternative structures expands the function and relevance of given nucleic acid regions and extends their biological function. These alternative nucleic acid structures can also pose a threat to the cell if their formation is not controlled and they form at "wrong" regions or too many at a specific time in the cell (Kosiol, Juranek, Brossart, Heine, & Paeschke, 2021; Richard & Manley, 2017; Shao & Zhang, 2020; Spiegel, Adhikari, & Balasubramanian, 2020; Svoboda & Di Cara, 2006). To prevent negative downstream consequences of "misregulated" alternative nucleic acid structures, their formation and unfolding is controlled by proteins. The most prominent alternative nucleic acids structures are hairpins, cruciform DNA, Z-DNA, and G-quadruplexes (Bochman, Paeschke, & Zakian, 2012). So far, only a few have been shown to be relevant *in vivo*. Among the best described alternative DNA and RNA conformation is the G-quadruplex structure (G4). G4 structures can form in guanine-rich sequences containing a specific sequence motif ($G\geq_2N_xG\geq_2N_yG\geq_2N_zG\geq_2$), called G4 motif. Because of this motif, the guanines self-assemble into (at least two) $\pi-\pi$ stacking subplanar guanine tetrads, which are stabilized by Hoogsteen hydrogen bonding and monovalent cations (Bochman et al., 2012; Burge, Parkinson, Hazel, Todd, & Neidle, 2006; Spiegel et al., 2020).

G4 motifs have been identified in all surveyed organisms (Huppert & Balasubramanian, 2005; Lavezzo et al., 2018; Marsico et al., 2019; Vannutelli, Belhamiti, Garant, Ouangraoua, & Perreault, 2020; Wu et al., 2021; Yadav et al., 2021; Yadav, Hemansi, Kim, Tuteja, & Yadav, 2017; Zyner et al., 2022). The genomic locations of G4 motifs are conserved and enriched at key genomic regions such as telomeres, promoters, splicing sites, origins of replication, untranslated regions of mRNAs and immunoglobulins switch regions, where they support cellular functions (Bohalova, Dobrovolna, Brazda, & Bidula, 2021; Capra, Paeschke, Singh, & Zakian, 2010; Huppert, 2010; Marsico et al., 2019; Wu et al., 2021). Therefore, the current model is that G4 structures are nucleic acid-based tools that support cellular functions.

In this model, specific G4s form based on exogenous or endogenous stimuli and support cellular pathways such as changes in gene expression (Bochman et al., 2012; Linke, Limmer, Juranek, Heine, & Paeschke, 2021; Lipps & Rhodes, 2009; Spiegel et al., 2020). In contrast to this regulatory function of G4s is the fact that G4 structures can, under certain conditions, also impair cellular functions and even lead to genome instability (De Magis et al., 2019; Gong et al., 2021; Hansel-Hertsch et al., 2020; Hui, Simeone, Zyner, Tannahill, & Balasubramanian, 2021, 2022; Paeschke et al., 2013; Paeschke, Capra, & Zakian, 2011; Wang et al., 2019). G4s can block the processivity of polymerases or form at incorrect times and locations on the DNA (RNA) as a protein loading hub to alter cellular changes (e.g., gene expression, epigenetic changes). It has been shown that persisting G4 structures can alter gene expression, splicing, mRNA abundance, stress response, telomerase activation, DNA damage accumulation and the efficiency of the DNA repair and replication machineries (Bryan, 2020; Kim, 2019; Kosiol et al., 2021; Robinson, Raguseo, Nuccio, Liano, & Di Antonio, 2021). Different proteins have been identified that impact G4 formation. These proteins can be grouped into two classes: G4 forming/stabilizing proteins and G4 unwinding proteins including helicases. So far, 25 eukaryotic helicases have been described that can unwind G4 structures. These helicases differ in directionality (5'-3' vs 3'-5'), their nucleic acid substrate (DNA vs RNA), and their mode in selection their targets. Furthermore, they differ in their G4-binding modes, as some helicases bind directly to the G4 structures, whereas others need a single-stranded tail in front of the G4s. Detailed structural analysis among helicases have shown that not only is their binding mode different, but the mechanism of G4 structures unwinding also differs among helicases (reviewed in (Caterino & Paeschke, 2021)).

Many processes in the cell depend on helicases. More than 31 DNA and 64 RNA helicases exist in humans (Umate, Tuteja, & Tuteja, 2011). Of these, 16 can bind to G4s. Most helicases can unwind G4s *in vitro,* and it is believed that more helicases will be identified that can unwind G4 structures *in vitro and vivo*. This raises two questions: (i) if nearly all helicases can unwind G4s, why is it worthwhile to characterize this function? (ii) If all helicases can unwind G4s *in vitro* does this still point to a special function or relevance *in vivo*. In our opinion, both questions can be answered with a clear "yes." Current experiments show that G4s have a function *in vivo* and that their formation and unfolding changes dynamically and depends on the cell type and cell state. This dynamic regulation is primarily dependent on helicases. As described above, without G4-unwinding helicases, G4s

accumulate in cells and lead to cellular defects (e.g., genome instability, stress, slow growth, apoptosis (Beauvarlet et al., 2019; Byrd et al., 2016; Lee et al., 2021; Qi et al., 2006; Sauer et al., 2019; Teng et al., 2021)). As most helicases can unwind G4s, this points to a significant role of G4s *in vivo*. By understanding which helicases can unwind G4s with which processivity and target preference, the function and relevance of G4 structures *in vivo* can be determined. The importance of helicase function at G4s is underlined by the current model that helicases support each other at G4s and can compensate for each other's loss at G4s. How helicase compensation at G4s is mediated and how they select their specific G4 targets is not currently clear. Detailed biochemical studies are required to understand if and how helicases unwind specific G4s. This knowledge is not only interesting for fundamental research to understand helicase function at G4s, but it is also of great interest for diagnostic and therapeutical aspects. Most human cancer cells have higher abundance of G4s, which may be connected to the mutational burden, cancer subtype generation and tumorigenesis (Biffi, Di Antonio, Tannahill, & Balasubramanian, 2014; Hansel-Hertsch et al., 2020; Hui et al., 2021, 2022; Kosiol et al., 2021). In some cancers, helicases that regulate G4s are mutated causing elevated G4s (Mohaghegh & Hickson, 2001; Suhasini & Brosh, 2013). A greater understanding on G4—helicase interaction will be essential to understand how G4s and helicases contribute to different cancer states and whether this can be used in the future as a diagnostic tool. In addition, the connection of G4s and helicases may also be relevant for novel therapeutic ideas. In recent years, chemical G4 ligands (e.g., PDS, BRACO-19, Telomestatin, CX5461) have been designed with the goal to stabilize G4s as a targeted approach for anti-cancer treatment (reviewed in (Kosiol et al., 2021; Sanchez-Martin, Soriano, & Garcia-Salcedo, 2021)). Multiple studies have shown that stabilized G4s cause alterations in the cancer cells that lead to reduced tumor growth and increased survival (Kosiol et al., 2021). So far, these ligands are very promising, but they can also cause many additional changes in the cells from undirected G4 stabilization. One interesting alternative approach could be to target specific G4s by modulating/blocking helicases (and their associated proteins) that contribute to G4 unwinding. This modulation of helicase activity will also increase G4 levels (of specific, selected G4s) and may also be useable as a therapeutic approach.

Multiple methods have been developed to study helicase function at G4s (reviewed in (Caterino & Paeschke, 2021)). We have limited the scope of this review on simple methods to study G4 unwinding by helicases using

a gel-based assay. We will explain in detail G4 target selection, G4 structure folding, controlling G4 structure formation and helicase activity assays.

2. Before you begin

Key to most *in vitro* assays is a detailed planning and small adjustments to experimental settings will be required in dependency on the selected helicase. Therefore, buffer preparation (pH, salt, source of NTP (most likely ATP)) and target selection can take quite some time, but once that is accomplished, data can be generated quickly. The following points needs to be considered and discussed before the start of the experiment:

- Selection of a helicase.

  Depending on your experimental setting, you must select a helicase to test on a given G4 substrate. Helicases are classified according to conserved sequence motifs into superfamilies (SF1-SF6). SF1 and SF2 are grouped based on similarities of two helicase domains (Fairman-Williams, Guenther, & Jankowsky, 2010). The SF1 helicase family shares a GDxxQ motif. SF2 helicases share structural similarities in the catalytic core. Based on the superfamily, you can deduce whether the helicase is a DNA or RNA helicase, which is the preferred NTP utilized for hydrolysis (e.g., ATP), and which unwinding polarity/directionality (5'-3, 3'-5') it employs. This information is essential to select and design targets for helicase activity assays.
- Purification of the helicase

  G4 unwinding by a helicase is a biochemical assay which requires recombinant expressed and purified helicase. The purification strategy is always dependent on the helicase. The helicase can be expressed and purified from *E. coli*, insect cells, yeasts or even in small amounts from cell culture cell that overexpress the helicase. Protocols how to express and purify different helicases can be found in the literature and adopted to the helicase of interest. For example, purification protocols for Pif1 or RecQ helicase members (Boule & Zakian, 2007; Gu, Masuda, & Kamiya, 2008; Karow, Chakraverty, & Hickson, 1997; Nickens & Bochman, 2021; Orren et al., 1999) or DHX36 and DDX5 (Chen et al., 2018; Choi, Dutta, Fielding, & Tan, 2010; Xing, Wang, & Tran, 2017; Yangyuoru, Bradburn, Liu, Xiao, & Russell, 2018) can be found in the literature. In most cases, it is important to understand whether an active unwinding process takes place or if the activity is passive (Benhalevy et al., 2017). This can either be monitored

by the amount of ATP hydrolyzed or by purifying mutated proteins that lack catalytic activity (e.g., mutations in the helicase core domains walker A or walker B box). For most cases described in the literature, the catalytic inactive helicases are expressed and purified with similar protocols to their active counterpart (Nickens & Bochman, 2021; Paeschke et al., 2013).

- Selection of DNA or RNA G4 targets

  It is also essential to select the target G4 structure to test your helicase. For this, it is advised to select either a standard G4-forming DNA or RNA sequence from the literature (for some examples that work in our hands see Table 1 or (Byrd & Raney, 2015)) or select a G4 motif from a genomic region or transcript, ideally of the same species of the helicase. A canonical G4 motif has four guanine tracts consisting of at least two guanines (see Fig. 1A for a cartoon of a G4 structure). These guanine tracts are separated by short intervening loop regions, which vary in their nucleotide composition. Different algorithms have successfully used this G4 motif to identify regions *in silico* that have a strong potential to fold into G4 structures (Brazda et al., 2019; Huppert & Balasubramanian, 2005; Lombardi & Londono-Vallejo, 2020; Miskiewicz, Sarzynska, & Szachniuk, 2021; Todd, Johnston, & Neidle, 2005). Different experimental findings also report G4 formation in guanine-rich regions that do not follow this canonical G4 motif (Jana, Mohr, Vianney, & Weisz, 2021). To map these G4 regions, a motif-independent screening tool has been developed that also identifies RNA G4 (Garant, Perreault, & Scott, 2017). Furthermore, polymerase stop assays and target-specific next generation sequencing approaches (e.g., chromatin immunoprecipitation) using G4-specific antibodies and probes have been performed in different organism that also experimentally determine G4 formation at specific DNA and RNA loci (Jamroskovic et al., 2019; Kwok, Marsico, & Balasubramanian, 2018; Marsico et al., 2019; Tu et al., 2021; Yang et al., 2018).
- Selection of control targets

  To estimate and compare helicase activity on G4 structures, a selection of control substrates is recommended. The choice of the control DNA or RNA regions depends on the scientific question. Most frequently, G-rich forked nucleic acid constructs were used as well as other secondary DNA or RNA structures such as hairpins or cruciform (Bochman et al., 2012; Ribeyre et al., 2009).
- Synthesizing DNA or RNA targets

  Selected regions can be ordered as standard unmodified oligonucleotides from commercial sources. Lyophilized oligonucleotides are reconstituted at

Table 1 Table provides examples of G-rich sequences that can fold G4 structures and have been used in the past for helicase unwinding experiments.

Sequence of G4 motif	Name of G4	Description	Topology
GGGGTTTTGGGGTTTTGGGGTTTTGGGG	Oxy Telo	Telomeric G4 sequence from *Stylonychia lemnea*	Antiparallel
GGGTTGGGTTGGGTTGGG	telo G4	Reduced loop size	Antiparallel
ACTGTCGTACTTGATATTTTGGGGTTTTGGGG	bi-Oxy G4	Bi-molecular telomeric G4 sequence from *Stylonychia lemnea*	Antiparallel
GGGGTGGGTAGGGTGGGTAA	c-MYC G4	G4 within c-MYC	Parallel
TTTCGGGCGGGCGCGAGGGAGGG	c-KIT G4	G4 within c-KIT	Parallel
TTTGGGAGGGAGAGGGGGDGGG	HIF-1alpha G4	G4 within HIF-1alpha	Parallel
TTTGGTTGGTGTGGTTGG	TBA G4	Thrombin binding G4 aptamer	Antiparallel
TGGACCAGACCTAGCAGCTATGGGGGAGCTGGGGAAGGTGGGAATGTGA	TP G4	Murine immunoglobulin switch sequence	Parallel
CCCAACCCAACCCTTCCC	rev_telo	Sequence use in helicase stop assay	No G4

Table provides sequences of G4 motif, name of the region used in the literature, description where this sequence origins from and the experimentally determined G4 topology.

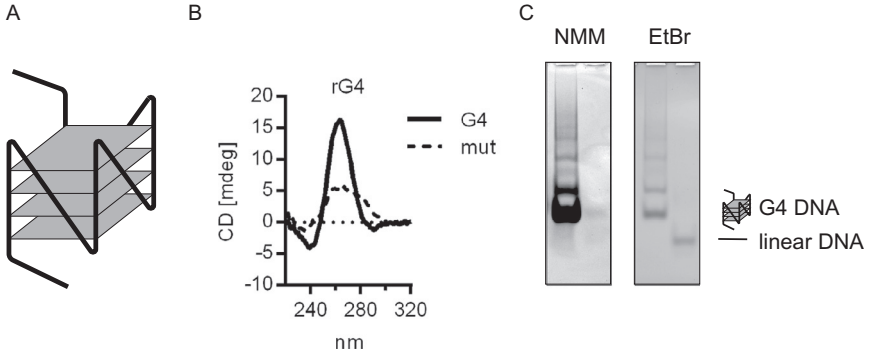

Fig. 1 Control of G4 formation. (A) Cartoon of a parallel G4 structure (B) CD spectra of a G4- and non-G4-forming oligodeoxynucleotide. (C) NMM- and ethidium bromide-(EtBr) stain of G4-forming oligodeoxynucleotide. EtBr gels detects all loaded nucleic acids. NMM gels visualizes only those nucleic acids that have a folded G4 structures. First lane G4, second lane control DNA (no G4 formation). Cartoon on the right indicates topology of the nucleic acid within the gel.

100 μM with ultrapure water. Oligonucleotides can be stored at −20 °C. RNA targets can be synthesized by *in vitro* transcription. For this. the target sequence will be in front of a T7 promoter and the RNA will be generated by reverse transcription. Due to the tight conformation of most G4s, we always add three adenines to the 5' end of each oligo. This renders the 5'-end free and available for end labeling instead of being buried within the G4. Also, we note that some helicases bind directly to the G4 (e.g., Pif1). Other helicases load in front of the G4 (e.g., DHX36 or BLM). These helicases require also an extension tail next to the G4. While designing these constructs that favor helicase binding and unwinding, please keep the directionality of your helicase in mind.

- Labeling of DNA or RNA target

  For later detection, DNA or RNA molecules need to be labeled. This protocol utilizes a radioactivity to label the DNA or RNA, however, alternative 5' or 3'-end labeling including biotinylation or addition of a fluorophore can be used. Labeling position needs to be carefully considered as to not hinder the formation of the G4 or affect helicase function.

3. Materials and equipment

3.1 General equipment

- Vertical polyacrylamide gel electrophoresis equipment (if using acrylamide gels)

- Horizontal gel electrophoresis equipment (if using agarose gels)
- Centrifuges (table-top) capable of cooling to 4 °C
- Incubators for 1.5 mL tubes (21–95 °C)
- Phosphoimager and phosphoimager screen (e.g. Typhoon FLA 7000) (alternative: X-ray films and developer). pH meter
- Circular dichroism (CD) instrument (e.g., Jasco-1500 spectropolarimeter)
- Quartz cell cuvette
- UV shadowing lamp
- Gel dryer (Biorad)
- Shaking incubators capable or heating (≥37 °C) and cooling (≤18 °C)

3.2 Reagents

- NaCl
- KCL
- Glycerol
- ß-Mercaptoethanol
- HEPES
- EDTA
- Tris
- HCl
- NaOH
- NaOAc
- $MgCl_2$
- Boric acid
- Agarose (if using agarose gels)
- Ethidium bromide
- 19:1 acrylamide:bis-acrylamide solution (PAA)
- Ammonium persulfate (APS) (if using acrylamide gels)
- *N,N,N',N'*-Tetramethylethylenediamine (TEMED) (if using acrylamide gels)
- Sodium dodecyl sulphate (SDS)
- Ammonium acetate
- Triton-X100
- Dithiothreitol (DTT)
- T4 polynucleotide kinase (PNK)
- G25 columns
- [sγ-^{32}P]ATP
- *N*-Methylmesoporphyrin IX (NMM)
- 10x TBE (1.3 M Tris (pH 7.6), 450 mM boric acid, 25 mM EDTA)
- Fresh 10% APS solution in water (if using acrylamide gels)

3.3 Oligonucleotides

Oligonucleotides can either be designed, taken from literature (Byrd & Raney, 2015) or be mined using biocomputational means (Brazda et al., 2019; Huppert & Balasubramanian, 2005; Lombardi & Londono-Vallejo, 2020; Miskiewicz et al., 2021; Todd et al., 2005). Examples are shown in Table 1.

4. Step-by-step method details

4.1 G4 formation

Different factors influence the formation of G4 structures including the type of salt, temperature, and the concentration of the oligonucleotide (Kim, Evans, Dubins, & Chalikian, 2015; Lane, Chaires, Gray, & Trent, 2008; You et al., 2017; Yuan et al., 2020). In general, use of K^+ leads to more stable G4s than Na^+, whereas Li^+ leads to less stable G4s (Bardin & Leroy, 2008; Kim et al., 2015). Of those ions, K^+ is discussed to be the more physiological relevant salt condition (Ghosh, Largy, & Gabelica, 2021; Zhang, Xu, Kumar, Zhang, & Wu, 2019).

As for many other protocols, there are different protocols described in the literature how to fold an G4 motif into a G4 structure *in vitro*. Here, we describe the two most common methods that were successfully used in our lab.

4.1.1 DNA G4 formation

DNA G4 formation

1. Selected DNA oligonucleotides (see above) were dissolved at 100 μM in G4 folding buffer (10 mM Tris (pH 7.5), 100 mM KCl, 1 mM EDTA). Depending on the experimental question KCl can be exchanged to NaCl or LiCl (see above). Once dissolved, we keep this as a stock, which is handy to freeze in aliquots at −20 °C. It is advised not to freeze/thaw the folded G4 oligonucleotides too often, which would prevent proper G4 formation.
2. Before the start of the experiment, the oligonucleotides will be diluted to 10 μM in G4 folding buffer.
3. Samples will be heat denatured for 10 min at 95 °C using a heating block.
4. Following denaturation, we slowly cool down samples to room temperature. We have achieved excellent results by decreasing the temperature

by 2 °C min^{-1} using either a PCR machine or temperature controlled incubators (Eppendorf thermomixer C).

5. Once the temperature reaches 21 °C, the G4 structures are folded properly.
6. Optional: To control for the efficiency of G4 formation, it is advised to separate the unfolded, partly folded and folded G4 structures from each other. This can be done by using vertical native gels (12% native acrylamide (19,1 acrylamide:bisacrylamide, 1x TBE, 1% APS, 0.1% TEMED). Gels will be run slowly using 10 V cm^{-1}. After ultraviolet shadowing, the correct size can be excised from the gel. Gel pieces can be cut into tiny pieces. Folded G4s are eluted overnight at 4 °C in TE (10 mM Tris, 1 mM EDTA pH 8.0) buffer. G4s are then ethanol-precipitated, dried and dissolved in water.

4.1.2 RNA G4 formation

1. Selected RNA G4 motifs were either synthesized or experimentally produced.
2. Selected RNA G4 oligonucleotides were dissolved at 2 μM in 10 mM Tris (pH 7.5) and 100 mM KCl (or NaCl/LiCl).
3. Samples will be heat denatured for 10 min at 95 °C using a heating block.
4. Following denaturation, slowly cool down the samples to room temperature. We have achieved excellent results by decreasing the temperature by 2 °C min^{-1} using either a PCR machine or temperature controlled incubators (e.g. Eppendorf Thermomixer C).
5. Once the temperature reaches 21 °C, the G4 structures are folded properly.

   Optional: To control for the efficiency of G4 formation, it is advised to separate unfolded, partly folded and fully folded G4 structures from each other. This can be done by using vertical native gels. After ultraviolet shadowing, the correct size can be excised from the gel. Gel pieces can be cut into tiny pieces. RNA fragment will be eluted overnight 4 °C in elution buffer (1 mM EDTA, 0.1% SDS and 0.5 M ammonium acetate). RNA G4s are then ethanol-precipitated, dried, and dissolved in water.

4.2 Control G4 structure formation

Different G4 structures conformations described in the literature can form parallel, anti-parallel, or as hybrid (Burge et al., 2006; Popenda, Miskiewicz, Sarzynska, Zok, & Szachniuk, 2020). It is known that protein binding and

helicase function may differ dependent on the G4 topology. Different methods have been developed to monitor the formation of G4 structures *in vitro*. Among the most commonly used are circular dichroism (CD) measurements (Del Villar-Guerra, Trent, & Chaires, 2018; Kejnovska, Renciuk, Palacky, & Vorlickova, 2019; Randazzo, Spada, & da Silva, 2013), *N*-methylmesoporphyrin (NMM) gels (Smith & Johnson, 2010), gel mobility changes in native gels (Moon & Jarstfer, 2010; Paeschke et al., 2013; Sun & Hurley, 2010), NMR (Lin, Dickerhoff, & Yang, 2019; Sket & Plavec, 2010; Webba da Silva, 2007), thermal melting experiments (Gray & Chaires, 2011), FRET (especially single molecule FRET (Juskowiak & Takenaka, 2006; Luo, Granzhan, Verga, & Mergny, 2021; Maleki, Budhathoki, Roy, & Balci, 2017)), and TDS spectra (UV basically (Dao, Haselsberger, Michel-Beyerle, & Phan, 2011; Mergny, Li, Lacroix, Amrane, & Chaires, 2005)). Here, we will describe CD and NMM gels in more detail.

4.2.1 CD

1. Either G4 folding buffer or water will be used as the blank in the spectropolarimeter (CD instrument). The spectral input of buffers, salts, and if required proteins were subtracted by using the software supplied with the instrument (Spectra Manager II Spectroscopy Software Suite).
2. Folded G4 structures (at least 2 μM, see above) will be pipetted into a 1 mL quartz cell cuvette with a path length of 1 mm.
3. CD spectra are recorded at 20 °C using a wavelength range of 220–320 nm.
4. Scanning speed should be 100 nm min^{-1} with a 1 s response time, 1 nm data pitch, and 1 nm bandwidth.
5. The measurement is repeated at least three times. Data will be presented as the average of three wavelength scans.
6. To analyze and interpret the data obtained by CD spectral analysis, distinct and characteristic maxima and minima peaks of G4 structures are essential. CD spectral features associated with specific G4 topologies, namely parallel G4 conformation have a distinct positive band at 264 nm and a relative shallow negative band at 245 nm; antiparallel G4 structures have a positive band at 295 nm and a negative band around 265 nm; hybrid G4 structures have two positive bands around 295 nm and 264 nm and a negative band around 245 nm. See Fig. 1A for an example of a parallel G4 structure.

4.2.2 N-*mesoporphyrin IX (NMM) native gel electrophoresis*

Different chemical probes (G4 ligands) have been generated that bind specifically to G4 structures. These G4 ligands bind and, in most cases, stabilize the G4 structure. These G4 ligands vary in their specificity toward G4s, and some exist that are either tagged or are fluorescent (Santos, Salgado, Cabrita, & Cruz, 2021; Umar, Ji, Chan, & Kwok, 2019). In this gel-based system. We use the G4-specific ligand NMM (K_D ~0.1–1 μM (Yett, Lin, Beseiso, Miao, & Yatsunyk, 2019)) to specifically stain parallel G4 structures in native TBE gels. thioflavin (ThT) also binds specifically to both parallel and antiparallel G4s and can be also used in this assay.

1. Prepare a native polyacrylamide TBE gel (1x TBE, 15% PAA (19,1), 1% APS, 0.1% TEMED). 15% is the optimal concentration to separate 10–100 bp.
2. After polymerization (30 min), assemble gel and add 1x TBE as running buffer to the chamber.
3. Wash wells thoroughly with 1x TBE to remove residual acrylamide.
4. Add to folded G4 structures (0.5 μg) 1x native loading dye (60 mM KCl, 10 mM Tris (pH 7.5), 50% (w/v) glycerol, 0.025% (w/v) xylene cyanol, 0.025% (w/v) bromophenol blue) and load samples in the wells.
5. Run electrophoresis for 90 min at 12 V cm^{-1}.
6. Prepare *N*-mesoporphyrin IX (NMM) stock solution. 4 mg NMM will be dissolved in 0.2 N HCL. Use dark tubes or wrap with aluminum foil and store the stock solution in the dark at room temperature.
7. After the electrophoresis is completed, stain the gel with 10 μg mL^{-1} NMM or 0.5 μM Thioflavin (ThT) in 1x G4 folding buffer for 15 min under agitation. Because NMM requires KCl, only KCl-containing staining buffers work for this reaction. If G4 structures are formed using either NaCl or LiCl, switch to a KCl-containing buffer. We keep the gels in the dark to avoid losing fluorescent signal.
8. G4 structures can be visualized using a gel-documentation system that can utilize excitation wavelengths of 399 nm (NMM) or 420 nm (ThT) (emission max: 610 and 487 nm, respectively). See Fig. 1B, left, for an example.
9. As a last step, we monitor all nucleic acids by staining with ethidium bromide. For this, gels will be incubated with 0.5 μg mL^{-1} ethidium bromide in 1x TBE for 15 min at room temperature. During this step we usually agitate the gels slowly.

10. Nucleic acids will be detected using a standard gel documentation system (e.g., BioRad, ChemiDoc) with an UV lamp (254 nm). See Fig. 1B, right, for an example.

4.3 Helicase activity assay

G4 structures can be unfolded by many helicases. Depending on the stability of the G4 structure and the length and position of an overhang (tail), helicase processivity differs among different helicase families and family members. Once the G4 structure is folded and controlled, established helicase assay for given helicase can be used. Different assays that measure helicase activity are possible with the generated substrates (e.g., FRET, ATP hydrolysis analysis, radioactive, and fluorescence gel-based assays). The buffers and timepoints described here are for Pif1 family members but work well for other helicases. In our lab, we have very good experience using radioactive helicase assays that will be analyzed on native gels. This has the advantage that small amounts of G4 structures and helicases are required for this assay.

1. Folded G4 DNA structures (e.g. telo G4, see Table 1) were 5' end labeled with ^{32}P using T4 PNK (NEB) according to the manufactures protocol.
2. After labeling free nucleotides were separated using a G25 column or similar to remove unincorporated radionucleotides.
3. Prepare 5x reaction buffer (100 mM Tris (pH 7.5), 200 mM NaCl, 500 $\mu g\,mL^{-1}$ BSA, 10 mM DTT).
4. Prepare helicase STOP buffer (17% Ficoll, 50 mM EDTA, 1 μM unlabeled single stranded DNA oligonucleotide (see Table 1 for example sequence matching telo G4) that is reverse complement to the G4 motif, 0.05% bromophenol blue and 0.05% xylene cyanol).
5. Prepare a 12% native polyacrylamide (19:1, 1x TBE, 1% APS, 0.1% TEMED) vertical gel.
6. To characterize the processivity of a given helicase on a G4 substrate the parameters in the helicase reaction can be altered. First, the concentration of the helicase and second the length/timing of the reaction. We will first (a) describe the reaction with altered helicase concentrations and second (b) the reaction with different incubation times of the helicases unwinding reaction.
7. Prepare seven tubes that contain: 1x reaction buffer, labeled DNA substrate (10 nM), 5 mM magnesium ions. The final reaction volume (after starting the reaction with ATP (see step 9) is 5 μL.

4.3.1 Effect of helicase concentration on G4 unwinding

1. Add to these seven tubes different concentrations of purified helicase. If you do not know how processive your helicase is, it is advised to choose a wide concentration range in the first experiments (e.g. 1 nM–100 mM) and narrow down the concentration in subsequent experiments to calculate unwinding parameters.
2. 1 out of these 7 samples will be collected without ATP as a reference to control for no helicase activity. Add 5 μL of STOP buffer and samples will be placed at 4 °C.
3. A second tube will be set to the site that will be used as a reference for full unwinding. This tube will be incubated for 10 min at 95 °C. The boiling step will linearize the G4. After boiling, 5 μL of STOP buffer must be added to prevent re-formation of the G4. Sample will be placed at 4 °C.
4. After setting the control samples, the reaction can be started using 4 mM ATP. Helicase unwinding will be performed at 30 °C in a thermal block or water bath
   a. Note, 30 °C is optimal for yeast Pif1. Other helicases from other organisms will perform better at higher temperatures, or, if unstable, need to be incubated at 4 °C for longer.
5. After 10 min (for less processive helicases this time can be extended to 30 min), the reaction will be stopped using 5 μL of STOP buffer.
6. Pre-run for 10 min a native gel ($10\,V\,cm^{-1}$) and wash wells after this thoroughly to remove soluble acrylamide and debits from wells.
7. Load total helicase reactions and run the gel for 30 min at $10\,V\,cm^{-1}$ in 1x TBE buffer.
8. Dry the gels using a vacuum gel drier and expose the dried gel to a phosphoimager plate for up to 24 h. Scan the phosphoimager screen using a phosphoimager. The gels can also be frozen at −20 °C for phosphoimager or film exposure. Note: to prevent gel cracking during drying or freezing, minimal amounts of TEMED (1%) should be used. Also, degassing of TBE is advised, as we observe better results.
9. Quantify helicase activity by measuring the densitometry for bands of the folded G4 and unfolded/linear substrate using ImageQuant, ImageJ, or similar software. Subtract the background from both bands. The controls, without ATP and the boiled sample, are set to 100% folded or unfolded, respectively, and the percentage of unwinding will be calculated based on these parameters (equation: (unwinding-background)/(control-background) * 100)

4.3.2 Time course for G4 unwinding

1. Add to all seven tubes 10 nM purified helicase.
2. As a 100% G4 folding control, take time-point 0. Here all oligos are 100% folded into a G4. The second control is the 100% unfolding control, which is prepared by boiling the tube for 10 min at 95 °C. STOP buffer will be added (5 μL) to these controls and kept at 4 °C.
3. After setting the control samples, the reaction can be started using 4 mM ATP. Helicase unwinding will be performed using a thermal block or water bath. Unwinding activity will be monitored over time.
4. If the processivity of your helicase on G4s is unknown, first monitor G4 unfolding over a longer range over time. We usually start with time points: 0 (not ATP),1, 2, 5, 10, 15, 30, and 60 min. Once the time frame of G4 unwinding is narrowed down, shorter and more detailed time slots can be selected (see Fig. 2A). All reaction will be stopped immediately using 5 μL of STOP buffer.
5. Pre-run for 10 min a native gel (10 V cm^{-1}) and afterwards wash wells thoroughly to remove soluble acrylamide and debits.
6. Load total helicase reaction and run reaction for 30 min at 10 V cm^{-1} in 1x TBE buffer.
7. Dry the gels using a vacuum gel drier and expose the dried gel to a phosphoimager plate as described in 3.1.1. (see Fig. 2A for an example).
8. Quantify helicase activity by measuring the densitometry for bands as described in 3.1.1. (see Fig. 2B for an example of the quantification of Fig. 2A).

Here, we describe a standard helicase assay for G4 DNA, but similar protocols work for G4 RNA. Since G4 can also form at the RNA level, it is noted

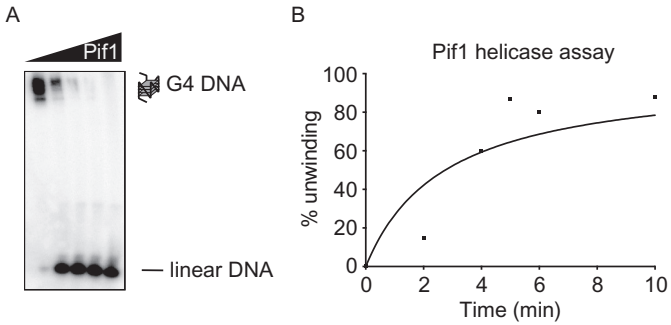

Fig. 2 G4 unwinding by Pif1 helicase (A), G4 unwinding over time was monitored by gel. Pif1 helicase action was monitored on Telo G4. (B) Quantification of unwinding reaction.

that to study G4 RNA unwinding by helicases, similar gel-based helicase unwinding protocols can be used. However, the amount and type of salt should be taken into consideration. Also, general good working practice for handling RNA should be observed, including using RNase-free reagents and plastic ware, reducing the heating times, and avoiding divalent cations.

Acknowledgments

We thank Philipp Schult for careful reading of the manuscript. Research in the Paeschke laboratory is fund by an ERC Stg Grant (638988-G4DSB) and by the Deutsche Forschungsgemeinschaft (DFG, German Research Foundation)—Project-ID 369799452—TRR237" as well as by the Deutsche Forschungsgemeinschaft (DFG, German Research Foundation) under Germany's Excellence Strategy—EXC2151—390873048.

References

Bardin, C., & Leroy, J. L. (2008). The formation pathway of tetramolecular G-quadruplexes. *Nucleic Acids Research*, *36*(2), 477–488.

Beauvarlet, J., Bensadoun, P., Darbo, E., Labrunie, G., Rousseau, B., Richard, E., et al. (2019). Modulation of the ATM/autophagy pathway by a G-quadruplex ligand tips the balance between senescence and apoptosis in cancer cells. *Nucleic Acids Research*, *47*(6), 2739–2756.

Benhalevy, D., Gupta, S. K., Danan, C. H., Ghosal, S., Sun, H. W., Kazemier, H. G., et al. (2017). The human CCHC-type zinc finger nucleic acid-binding protein binds G-rich elements in target mRNA coding sequences and promotes translation. *Cell Reports*, *18*(12), 2979–2990.

Biffi, G., Di Antonio, M., Tannahill, D., & Balasubramanian, S. (2014). Visualization and selective chemical targeting of RNA G-quadruplex structures in the cytoplasm of human cells. *Nature Chemistry*, *6*(1), 75–80.

Bochman, M. L., Paeschke, K., & Zakian, V. A. (2012). DNA secondary structures: Stability and function of G-quadruplex structures. *Nature Reviews. Genetics*, *13*(11), 770–780.

Bohalova, N., Dobrovolna, M., Brazda, V., & Bidula, S. (2021). Conservation and over-representation of G-quadruplex sequences in regulatory regions of mitochondrial DNA across distinct taxonomic sub-groups. *Biochimie*, *194*, 28–34.

Boule, J. B., & Zakian, V. A. (2007). The yeast Pif1p DNA helicase preferentially unwinds RNA DNA substrates. *Nucleic Acids Research*, *35*(17), 5809–5818.

Brazda, V., Kolomaznik, J., Lysek, J., Bartas, M., Fojta, M., Stastny, J., et al. (2019). G4Hunter web application: A web server for G-quadruplex prediction. *Bioinformatics*, *35*(18), 3493–3495.

Bryan, T. M. (2020). G-quadruplexes at telomeres: Friend or foe? *Molecules*, *25*(16).

Burge, S., Parkinson, G. N., Hazel, P., Todd, A. K., & Neidle, S. (2006). Quadruplex DNA: Sequence, topology and structure. *Nucleic Acids Research*, *34*(19), 5402–5415.

Byrd, A. K., & Raney, K. D. (2015). A parallel quadruplex DNA is bound tightly but unfolded slowly by pif1 helicase. *The Journal of Biological Chemistry*, *290*(10), 6482–6494.

Byrd, A. K., Zybailov, B. L., Maddukuri, L., Gao, J., Marecki, J. C., Jaiswal, M., et al. (2016). Evidence that G-quadruplex DNA accumulates in the cytoplasm and participates in stress granule assembly in response to oxidative stress. *The Journal of Biological Chemistry*, *291*(34), 18041–18057.

Capra, J. A., Paeschke, K., Singh, M., & Zakian, V. A. (2010). G-quadruplex DNA sequences are evolutionarily conserved and associated with distinct genomic features in Saccharomyces cerevisiae. *PLoS Computational Biology*, *6*(7), e1000861.

Caterino, M., & Paeschke, K. (2021). Action and function of helicases on RNA G-quadruplexes. *Methods*.

Chen, M. C., Tippana, R., Demeshkina, N. A., Murat, P., Balasubramanian, S., Myong, S., et al. (2018). Structural basis of G-quadruplex unfolding by the DEAH/RHA helicase DHX36. *Nature*, *558*(7710), 465–469.

Choi, Y. W., Dutta, S., Fielding, B. C., & Tan, Y. J. (2010). Expression, purification and preliminary crystallographic analysis of recombinant human DEAD-box polypeptide 5. *Acta Crystallographica. Section F, Structural Biology and Crystallization Communications*, *66*(Pt. 2), 192–194.

Dao, N. T., Haselsberger, R., Michel-Beyerle, M. E., & Phan, A. T. (2011). Following G-quadruplex formation by its intrinsic fluorescence. *FEBS Letters*, *585*(24), 3969–3977.

De Magis, A., Manzo, S. G., Russo, M., Marinello, J., Morigi, R., Sordet, O., et al. (2019). DNA damage and genome instability by G-quadruplex ligands are mediated by R loops in human cancer cells. *Proceedings of the National Academy of Sciences of the United States of America*, *116*(3), 816–825.

Del Villar-Guerra, R., Trent, J. O., & Chaires, J. B. (2018). G-quadruplex secondary structure obtained from circular dichroism spectroscopy. *Angewandte Chemie (International Edition in English)*, *57*(24), 7171–7175.

Fairman-Williams, M. E., Guenther, U. P., & Jankowsky, E. (2010). SF1 and SF2 helicases: Family matters. *Current Opinion in Structural Biology*, *20*.

Garant, J. M., Perreault, J. P., & Scott, M. S. (2017). Motif independent identification of potential RNA G-quadruplexes by G4RNA screener. *Bioinformatics*, *33*(22), 3532–3537.

Ghosh, A., Largy, E., & Gabelica, V. (2021). DNA G-quadruplexes for native mass spectrometry in potassium: A database of validated structures in electrospray-compatible conditions. *Nucleic Acids Research*, *49*(4), 2333–2345.

Gong, J. Y., Wen, C. J., Tang, M. L., Duan, R. F., Chen, J. N., Zhang, J. Y., et al. (2021). G-quadruplex structural variations in human genome associated with single-nucleotide variations and their impact on gene activity. *Proceedings of the National Academy of Sciences of the United States of America*, *118*(21).

Gray, R. D., & Chaires, J. B. (2011). Analysis of multidimensional G-quadruplex melting curves. *Current Protocols in Nucleic Acid Chemistry*, *17*. Unit 17.4.

Gu, Y., Masuda, Y., & Kamiya, K. (2008). Biochemical analysis of human PIF1 helicase and functions of its N-terminal domain. *Nucleic Acids Research*, *36*(19), 6295–6308.

Hansel-Hertsch, R., Simeone, A., Shea, A., Hui, W. W. I., Zyner, K. G., Marsico, G., et al. (2020). Landscape of G-quadruplex DNA structural regions in breast cancer. *Nature Genetics*, *52*(9), 878–883.

Hui, W. W. I., Simeone, A., Zyner, K. G., Tannahill, D., & Balasubramanian, S. (2021). Single-cell mapping of DNA G-quadruplex structures in human cancer cells. *Scientific Reports*, *11*(1), 23641.

Hui, W. W. I., Simeone, A., Zyner, K. G., Tannahill, D., & Balasubramanian, S. (2022). Publisher correction: Single-cell mapping of DNA G-quadruplex structures in human cancer cells. *Scientific Reports*, *12*(1), 908.

Huppert, J. L. (2010). Structure, location and interactions of G-quadruplexes. *The FEBS Journal*, *277*(17), 3452–3458.

Huppert, J. L., & Balasubramanian, S. (2005). Prevalence of quadruplexes in the human genome. *Nucleic Acids Research*, *33*(9), 2908–2916.

Jamroskovic, J., Obi, I., Movahedi, A., Chand, K., Chorell, E., & Sabouri, N. (2019). Identification of putative G-quadruplex DNA structures in S. pombe genome by quantitative PCR stop assay. *DNA Repair (Amst)*, *82*, 102678.

Jana, J., Mohr, S., Vianney, Y. M., & Weisz, K. (2021). Structural motifs and intramolecular interactions in non-canonical G-quadruplexes. *RSC Chemical Biology*, *2*(2), 338–353.
Juskowiak, B., & Takenaka, S. (2006). Fluorescence resonance energy transfer in the studies of guanine quadruplexes. *Methods in Molecular Biology*, *335*, 311–341.
Karow, J. K., Chakraverty, R. K., & Hickson, I. D. (1997). The Bloom's syndrome gene product is a 3'-5' DNA helicase. *The Journal of Biological Chemistry*, *272*(49), 30611–30614.
Kejnovska, I., Renciuk, D., Palacky, J., & Vorlickova, M. (2019). CD study of the G-quadruplex conformation. *Methods in Molecular Biology*, *2035*, 25–44.
Kim, N. (2019). The interplay between G-quadruplex and transcription. *Current Medicinal Chemistry*, *26*(16), 2898–2917.
Kim, B. G., Evans, H. M., Dubins, D. N., & Chalikian, T. V. (2015). Effects of salt on the stability of a G-quadruplex from the human c-MYC promoter. *Biochemistry*, *54*(22), 3420–3430.
Kosiol, N., Juranek, S., Brossart, P., Heine, A., & Paeschke, K. (2021). G-quadruplexes: A promising target for cancer therapy. *Molecular Cancer*, *20*(1), 40.
Kwok, C. K., Marsico, G., & Balasubramanian, S. (2018). Detecting RNA G-quadruplexes (rG4s) in the transcriptome. *Cold Spring Harbor Perspectives in Biology*, *10*(7).
Lane, A. N., Chaires, J. B., Gray, R. D., & Trent, J. O. (2008). Stability and kinetics of G-quadruplex structures. *Nucleic Acids Research*, *36*(17), 5482–5515.
Lavezzo, E., Berselli, M., Frasson, I., Perrone, R., Palu, G., Brazzale, A. R., et al. (2018). G-quadruplex forming sequences in the genome of all known human viruses: A comprehensive guide. *PLoS Computational Biology*, *14*(12), e1006675.
Lee, W. T. C., Yin, Y., Morten, M. J., Tonzi, P., Gwo, P. P., Odermatt, D. C., et al. (2021). Single-molecule imaging reveals replication fork coupled formation of G-quadruplex structures hinders local replication stress signaling. *Nature Communications*, *12*(1), 2525.
Lin, C., Dickerhoff, J., & Yang, D. (2019). NMR studies of G-quadruplex structures and G-quadruplex-interactive compounds. *Methods in Molecular Biology*, *2035*, 157–176.
Linke, R., Limmer, M., Juranek, S. A., Heine, A., & Paeschke, K. (2021). The relevance of G-quadruplexes for DNA repair. *International Journal of Molecular Sciences*, *22*(22).
Lipps, H. J., & Rhodes, D. (2009). G-quadruplex structures: In vivo evidence and function. *Trends in Cell Biology*, *19*(8), 414–422.
Lombardi, E. P., & Londono-Vallejo, A. (2020). A guide to computational methods for G-quadruplex prediction. *Nucleic Acids Research*, *48*(3), 1603.
Luo, Y., Granzhan, A., Verga, D., & Mergny, J. L. (2021). FRET-MC: A fluorescence melting competition assay for studying G4 structures in vitro. *Biopolymers*, *112*(4), e23415.
Maleki, P., Budhathoki, J. B., Roy, W. A., & Balci, H. (2017). A practical guide to studying G-quadruplex structures using single-molecule FRET. *Molecular Genetics and Genomics*, *292*(3), 483–498.
Marsico, G., Chambers, V. S., Sahakyan, A. B., McCauley, P., Boutell, J. M., Antonio, M. D., et al. (2019). Whole genome experimental maps of DNA G-quadruplexes in multiple species. *Nucleic Acids Research*, *47*(8), 3862–3874.
Mergny, J. L., Li, J., Lacroix, L., Amrane, S., & Chaires, J. B. (2005). Thermal difference spectra: A specific signature for nucleic acid structures. *Nucleic Acids Research*, *33*(16), e138.
Miskiewicz, J., Sarzynska, J., & Szachniuk, M. (2021). How bioinformatics resources work with G4 RNAs. *Briefings in Bioinformatics*, *22*(3).
Mohaghegh, P., & Hickson, I. D. (2001). DNA helicase deficiencies associated with cancer predisposition and premature ageing disorders. *Human Molecular Genetics*, *10*(7), 741–746.
Moon, I. K., & Jarstfer, M. B. (2010). Preparation of G-quartet structures and detection by native gel electrophoresis. *Methods in Molecular Biology*, *608*, 51–63.
Nickens, D. G., & Bochman, M. L. (2021). Characterization of the telomerase modulating activities of yeast DNA helicases. *Methods in Enzymology*, *661*, 327–342.

Orren, D. K., Brosh, R. M., Jr., Nehlin, J. O., Machwe, A., Gray, M. D., & Bohr, V. A. (1999). Enzymatic and DNA binding properties of purified WRN protein: High affinity binding to single-stranded DNA but not to DNA damage induced by 4NQO. *Nucleic Acids Research*, *27*(17), 3557–3566.

Paeschke, K., Bochman, M. L., Garcia, P. D., Cejka, P., Friedman, K. L., Kowalczykowski, S. C., et al. (2013). Pif1 family helicases suppress genome instability at G-quadruplex motifs. *Nature*, *497*(7450), 458–462.

Paeschke, K., Capra, J. A., & Zakian, V. A. (2011). DNA replication through G-quadruplex motifs is promoted by the Saccharomyces cerevisiae Pif1 DNA helicase. *Cell*, *145*(5), 678–691.

Popenda, M., Miskiewicz, J., Sarzynska, J., Zok, T., & Szachniuk, M. (2020). Topology-based classification of tetrads and quadruplex structures. *Bioinformatics*, *36*(4), 1129–1134.

Qi, H., Lin, C. P., Fu, X., Wood, L. M., Liu, A. A., Tsai, Y. C., et al. (2006). G-quadruplexes induce apoptosis in tumor cells. *Cancer Research*, *66*(24), 11808–11816.

Randazzo, A., Spada, G. P., & da Silva, M. W. (2013). Circular dichroism of quadruplex structures. *Topics in Current Chemistry*, *330*, 67–86.

Ribeyre, C., Lopes, J., Boule, J. B., Piazza, A., Guedin, A., Zakian, V. A., et al. (2009). The yeast Pif1 helicase prevents genomic instability caused by G-quadruplex-forming CEB1 sequences in vivo. *PLoS Genetics*, *5*(5), e1000475.

Richard, P., & Manley, J. L. (2017). R loops and links to human disease. *Journal of Molecular Biology*, *429*(21), 3168–3180.

Robinson, J., Raguseo, F., Nuccio, S. P., Liano, D., & Di Antonio, M. (2021). DNA G-quadruplex structures: More than simple roadblocks to transcription? *Nucleic Acids Research*, *49*(15), 8419–8431.

Sanchez-Martin, V., Soriano, M., & Garcia-Salcedo, J. A. (2021). Quadruplex ligands in cancer therapy. *Cancers (Basel)*, *13*(13).

Santos, T., Salgado, G. F., Cabrita, E. J., & Cruz, C. (2021). G-quadruplexes and their ligands: Biophysical methods to unravel G-quadruplex/ligand interactions. *Pharmaceuticals (Basel)*, *14*(8).

Sauer, M., Juranek, S. A., Marks, J., De Magis, A., Kazemier, H. G., Hilbig, D., et al. (2019). DHX36 prevents the accumulation of translationally inactive mRNAs with G4-structures in untranslated regions. *Nature Communications*, *10*(1), 2421.

Shao, Y., & Zhang, Q. C. (2020). Targeting RNA structures in diseases with small molecules. *Essays in Biochemistry*, *64*(6), 955–966.

Shapiro, J. A. (2009). Revisiting the central dogma in the 21st century. *Annals of the New York Academy of Sciences*, *1178*, 6–28.

Sket, P., & Plavec, J. (2010). Tetramolecular DNA quadruplexes in solution: Insights into structural diversity and cation movement. *Journal of the American Chemical Society*, *132*(36), 12724–12732.

Smith, J. S., & Johnson, F. B. (2010). Isolation of G-quadruplex DNA using NMM-sepharose affinity chromatography. *Methods in Molecular Biology*, *608*, 207–221.

Spiegel, J., Adhikari, S., & Balasubramanian, S. (2020). The structure and function of DNA G-quadruplexes. *Trends Chemistry*, *2*(2), 123–136.

Suhasini, A. N., & Brosh, R. M., Jr. (2013). DNA helicases associated with genetic instability, cancer, and aging. *Advances in Experimental Medicine and Biology*, *767*, 123–144.

Sun, D., & Hurley, L. H. (2010). Biochemical techniques for the characterization of G-quadruplex structures: EMSA, DMS footprinting, and DNA polymerase stop assay. *Methods in Molecular Biology*, *608*, 65–79.

Svoboda, P., & Di Cara, A. (2006). Hairpin RNA: A secondary structure of primary importance. *Cellular and Molecular Life Sciences*, *63*(7-8), 901–908.

Teng, Y. C., Sundaresan, A., O'Hara, R., Gant, V. U., Li, M., Martire, S., et al. (2021). ATRX promotes heterochromatin formation to protect cells from G-quadruplex DNA-mediated stress. *Nature Communications*, *12*(1), 3887.

Todd, A. K., Johnston, M., & Neidle, S. (2005). Highly prevalent putative quadruplex sequence motifs in human DNA. *Nucleic Acids Research*, *33*(9), 2901–2907.

Tu, J., Duan, M., Liu, W., Lu, N., Zhou, Y., Sun, X., et al. (2021). Direct genome-wide identification of G-quadruplex structures by whole-genome resequencing. *Nature Communications*, *12*(1), 6014.

Umar, M. I., Ji, D., Chan, C. Y., & Kwok, C. K. (2019). G-quadruplex-based fluorescent turn-on ligands and aptamers: From development to applications. *Molecules*, *24*(13).

Umate, P., Tuteja, N., & Tuteja, R. (2011). Genome-wide comprehensive analysis of human helicases. *Communicative & Integrative Biology*, *4*(1), 118–137.

Vannutelli, A., Belhamiti, S., Garant, J. M., Ouangraoua, A., & Perreault, J. P. (2020). Where are G-quadruplexes located in the human transcriptome? *NAR Genomics and Bioinformatics*, *2*(2), lqaa035.

Wang, Y., Yang, J., Wild, A. T., Wu, W. H., Shah, R., Danussi, C., et al. (2019). G-quadruplex DNA drives genomic instability and represents a targetable molecular abnormality in ATRX-deficient malignant glioma. *Nature Communications*, *10*(1), 943.

Webba da Silva, M. (2007). NMR methods for studying quadruplex nucleic acids. *Methods*, *43*(4), 264–277.

Wu, M. T., & D'Souza, V. (2020). Alternate RNA structures. *Cold Spring Harbor Perspectives in Biology*, *12*(1).

Wu, F., Niu, K., Cui, Y., Li, C., Lyu, M., Ren, Y., et al. (2021). Genome-wide analysis of DNA G-quadruplex motifs across 37 species provides insights into G4 evolution. *Communications Biology*, *4*(1), 98.

Xing, Z., Wang, S., & Tran, E. J. (2017). Characterization of the mammalian DEAD-box protein DDX5 reveals functional conservation with S. cerevisiae ortholog Dbp2 in transcriptional control and glucose metabolism. *RNA*, *23*(7), 1125–1138.

Yadav, V., Hemansi, Kim, N., Tuteja, N., & Yadav, P. (2017). Quadruplex in plants: A ubiquitous regulatory element and its biological relevance. *Frontiers in Plant Science*, *8*, 1163.

Yadav, P., Kim, N., Kumari, M., Verma, S., Sharma, T. K., Yadav, V., et al. (2021). G-quadruplex structures in bacteria: Biological relevance and potential as an antimicrobial target. *Journal of Bacteriology*, *203*(13), e0057720.

Yang, S. Y., Lejault, P., Chevrier, S., Boidot, R., Robertson, A. G., Wong, J. M. Y., et al. (2018). Transcriptome-wide identification of transient RNA G-quadruplexes in human cells. *Nature Communications*, *9*(1), 4730.

Yangyuoru, P. M., Bradburn, D. A., Liu, Z., Xiao, T. S., & Russell, R. (2018). The G-quadruplex (G4) resolvase DHX36 efficiently and specifically disrupts DNA G4s via a translocation-based helicase mechanism. *The Journal of Biological Chemistry*, *293*(6), 1924–1932.

Yett, A., Lin, L. Y., Beseiso, D., Miao, J., & Yatsunyk, L. A. (2019). N-methyl mesoporphyrin IX as a highly selective light-up probe for G-quadruplex DNA. *Journal of Porphyrins and Phthalocyanines*, *23*(11n12), 1195–1215.

You, J., Li, H., Lu, X. M., Li, W., Wang, P. Y., Dou, S. X., et al. (2017). Effects of monovalent cations on folding kinetics of G-quadruplexes. *Bioscience Reports*, *37*(4).

Yuan, W. F., Wan, L. Y., Peng, H., Zhong, Y. M., Cai, W. L., Zhang, Y. Q., et al. (2020). The influencing factors and functions of DNA G-quadruplexes. *Cell Biochemistry and Function*, *38*(5), 524–532.

Zhang, M. L., Xu, Y. P., Kumar, A., Zhang, Y., & Wu, W. Q. (2019). Studying the potassium-induced G-quadruplex DNA folding process using microscale thermophoresis. *Biochemistry*, *58*(38), 3955–3959.

Zyner, K. G., Simeone, A., Flynn, S. M., Doyle, C., Marsico, G., Adhikari, S., et al. (2022). G-quadruplex DNA structures in human stem cells and differentiation. *Nature Communications*, *13*(1), 142.